doi:10.14311/ppt.2025.1.61
Plasma Physics and Technology **12**(1):61–66, 2025

EXPERIMENTAL CHARACTERIZATION OF PRE-STRIKE ARC DURATION OF A MV-LBS USING N_2/CO_2: INFLUENCE OF CLOSING SPEED, PRESSURE AND MIXING RATIO

M. Castiñeira Suárez[a,*], F. Mingers[a], W. Leterme[a], M. Schaak[b], K. Ermeler[c]

[a] *IAEW at RWTH Aachen University, Schinkelstr. 2, 52056 Aachen, Germany*
[b] *Siemens AG, Smart Infrastructure, Carl-Benz-Str. 22, 60386 Frankfurt am Main, Germany*
[c] *Siemens AG, Smart Infrastructure, Nonnendammallee 104, 13629 Berlin, Germany*
[*] m.suarez@iaew.rwth-aachen.de

Abstract. Short-circuit current making in a medium voltage load-break switch using N_2/CO_2 is expected to result in longer pre-strike arcs compared to SF_6, due to lower dielectric strength, leading to increased contact degradation. Measures to limit impact of pre-strike arc on the contact system are needed. This paper aims to experimentally investigate the influence of closing speed, filling pressure and mixing ratio on pre-strike arc duration towards increasing contact system life time.

Keywords: load break switch, medium voltage, SF_6 alternatives, pre-strike arc, short-circuit current making.

1. Introduction

Medium voltage (MV) load break switches (LBSs) are the main switchgear component used in secondary distribution grids. They are frequently used in ring main units (RMUs) for interruption of load currents up to 1.25 kA and ensuring a safe insulating distance in open circuit conditions. The use of SF_6 allows for a compact design thanks to its high dielectric strength and good arc-quenching properties. However, SF_6 is the strongest green-house gas with a global warming potential of 23 500 [1]. Substitution of SF_6 by eco-friendly alternatives entails challenges during the short-circuit currrent making (SCCM) process, due to their comparatively lower dielectric strength.

During the current making process, an electric (pre-strike) arc is ignited across the open contacts of the switch. A fraction of the energy dissipated by the arc is absorbed by the contacts. Current making can take place under fault conditions of the grid, which leads to short-circuit currents in the range of some tens of kA. Such high-current pre-strike arcs can lead to melting of the contact surfaces. Upon reaching closed position, the molten surfaces of the contacts cool down and solidify, potentially resulting in contact welding and failure to reopen. According to IEC 62271-103, the LBS must be able to making short-circuit currents and be subsequently manually reopened.

The SCCM process is expected to result in more severe contact degradation when alternative gases are used. Due to their lower dielectric strength [2], arc ignition takes place at a greater contact distance, thus leading to longer pre-strike arcs and higher dissipated energy. To limit the impact of pre-strike arcs in the contact system of an eco-friendly LBS, measures aiming to reduce pre-strike arc duration are needed.

In [3–5], the SCCM process was investigated in a LBS using air at ambient pressure. The pre-strike arc interval was found to be the most destructive part of the SCCM process. Increased contact degradation was observed for longer pre-strike arc durations. Increasing the closing speed and filling pressure are suggested as possible approaches for reducing contact degradation.

Most published work on the topic of SF_6-free MV-LBSs focuses on interruption performance. In particular, a sufficient load current interruption capability was demonstrated for a LBS using N_2/CO_2 gas mixtures in combination with forced cooling through a PTFE nozzle, and the required design criteria was derived in [6–8]. The influence of SCCM on the service life of a LBS using N_2/CO_2 has yet to be investigated.

The objective of this paper is to experimentally investigate the influence of relevant parameters towards limiting pre-strike arc duration when using N_2/CO_2 gas mixtures. These parameters aim to impact arc duration directly (closing speed) or indirectly, by increasing the dielectric strength of the filling gas and therefore delaying arc ignition (filling pressure, mixing ratio). The device under test (DUT) consists of a model switch based on design criteria derived in [6–8] for a LBS in the 24 kV level.

2. Method

This work experimentally evaluates the influence of three parameters on pre-strike arc duration, namely closing speed (v_c), filling pressure (p_f) and % of CO_2 in a N_2/CO_2 gas mixture (r_{CO2}). The experimental setup enables evaluation of these parameters on pre-strike arc duration (t_{pa}) and contact distance at the moment of arc ignition (d). A full factorial design

of the parameters shown in Table 1 is considered, resulting in 45 variations. Variation of r_{CO2} requires extraction of the existing gas inside the vessel, before refilling with the corresponding gas mixture to be investigated. This process is time intensive. For this reason, the sequence of experiments is organized based on block randomization, where v_c and p_f are randomized in 15 blocks of 3 parameter combinations at constant r_{CO2} (Table 2).

	Parameter values
v_c in m/s	1 - 2 - 3 - 4 - 5
p_f in bar	1.4 - 1.8 - 2.2
r_{CO2} in % CO_2	10 - 40 - 70

Table 1. Range of parameters investigated

Block	r_{CO2}	v_c	p_f
1	40	3	1.4
1	40	1	1.8
1	40	5	2.2

Table 2. Exemplary randomized block for $r_{CO2} = 40\,\%$.

2.1. Short-circuit current making

Standard IEC-62271-101 defines three intervals during the SCCM process (Figure 1). The high-voltage interval starts at t_0, when the moving contact is released. Grid voltage $u(t)$ can measured between the open contacts. Breakdown voltage U_{bd} is reduced as contact distance decreases. The pre-strike interval starts at t_1, when U_{bd} decreases below $u(t)$ and breakdown between the contacts leads to ignition of the pre-strike arc. The short-circuit current $i(t)$ starts flowing between the arcing contacts. The latching interval starts at t_2, when galvanic contact is reached, and ends at the final closed position (t_3). This interval can be further divided into two stages. A first stage where only arcing contacts are touching, and a second stage starting when galvanic contact of the main contacts is reached (somewhere between t_2 and t_3). At this point, short-circuit current starts flowing through both sets of contacts.

The point in time of pre-strike arc ignition relative to $u(t)$ determines pre-strike duration. Arc ignition at $\hat{U}$ (Figure 1) results in longest pre-strike arc duration and therefore highest arc energy dissipated between the contacts [5]. Arc ignition near voltage zero implies a smaller contact distance at the moment of breakdown, and therefore shorter arcs. The later case results in asymmetrical currents and higher electrodynamic stress on the LBS, which could potentially increase the risk of contact bouncing during the latching interval and have an influence on contact welding. This paper focuses on the pre-strike arc. For this reason, arc ignition at the peak value of $u(t)$ is considered.

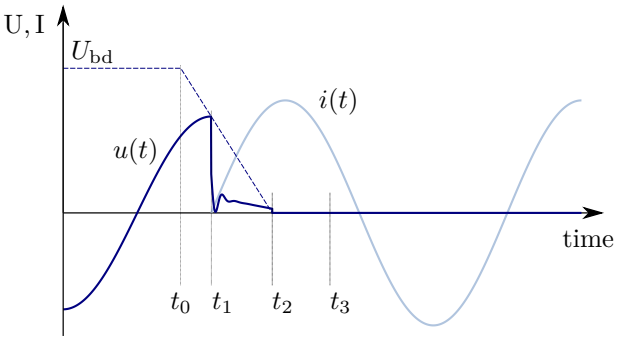

Figure 1. Schematic representation of voltage and current during SCCM.

In real applications, contact erosion due to high-short-circuit current arcs alters contact geometry and surface roughness, which can lead to increasing pre-strike arc durations for subsequent SCCM operations. Variations in contact geometry can consequently influence the electric field distribution, thereby leading to earlier arc ignition. Moreover, the loss of contact material may result in delayed galvanic contact. Due to the increasing arc duration on subsequent SCCM operations, an increased dissipated energy is also expected. Therefore, the influence of pre-strike arc on subsequent making operations is critical and must be considered when evaluating contact degradation during SCCM. However, the aim of this work is to exclusively investigate the influence of v_c, p_f and r_{CO2} on pre-strike arc duration. To limit contact degradation and minimize the number of contacts required while enabling repeated tests for the same parameter variation, a test circuit providing currents in the mA range is used.

2.1.1. Test setup and evaluation of results

To generate the required test voltage, an RC circuit connected in series with the DUT is used, where $R = 5\,\mathrm{M\Omega}$ and $C = 5.78\,\mu\mathrm{F}$. A half-wave rectifier is used to charge C to $U_0 = \{21.4 \pm 0.3\}\,\mathrm{kV}$, slightly above the corresponding peak voltage in the 24 kV level (20 kV).

Voltage across the contacts of the DUT is measured using a PVM-5 Northstar voltage divider. Distance traveled by the moving pin contact is measured with a IL-300 Keyence laser sensor (30 µm repeatability), connected to an IL-1000 Keyence amplifier unit. Tests are initiated by closing the contacts of DUT.

Voltage and travel measurements for an exemplary test are shown in Figure 2. The moment of arc ignition (t_1) takes place at $t = 0\,\mathrm{ms}$, when U_0 leads to breakdown between the contacts. Due to the resulting low current (in the range of several mA) the arc cannot be sustained and is immediately extinguished, leading to a subsequent voltage rise. Following the first breakdown, four voltage drops can be observed. The point in time of the last voltage drop ($t \approx 1.67\,\mathrm{ms}$)

coincides with the travel measurement corresponding to the moment of galvanic contact (t_2), once the pin contact has traveled $\Delta z_{gc} \approx 83\,\text{mm}$. The resulting t_{pa} is calculated as $t_{pa} = t_2 - t_1$. For each parameter combination, ten making operations are performed.

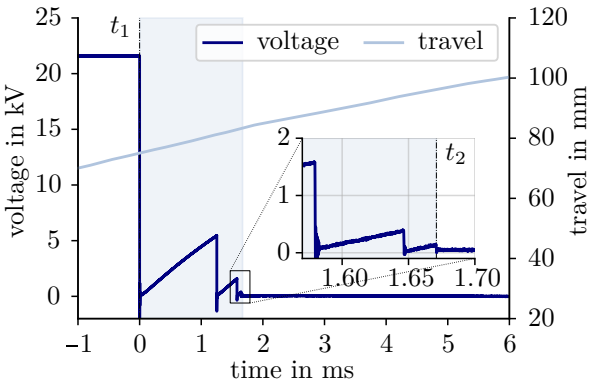

Figure 2. Voltage and travel signal measurements for an exemplary test

Pre-strike arc duration is used to calculate the prospective arc energy W_{pa}. In [9], contact mass loss is presented as a function of the effective arc energy into the surface of the contacts (Equation 1).

$$W_{pa} = \int_{t_1}^{t_2} \Delta U_{fall} \cdot i(t)\,dt \tag{1}$$

In this contribution, arc energy based on this approach is normalized to peak value of the symmetric short-circuit current ($W_{pa}/\hat{I}$). The effective voltage drop in the electrode fall region ΔU_{fall} (considering cathode and anode) is assumed to be approximately 17 V for WCu 80/20 contacts and currents between 3 and 45 kA [9, 10]. Additionally, contact distance at the moment of breakdown d and voltage measured before arc ignition U_{bd} are used to calculate the breakdown field strength between the contacts ($E_{bd} = U_{bd}/d$).

2.2. Model switch

The DUT is based on a linear puffer-type LBS (Figure 3). It consists of a moving pin and fixed tulip contact system made of WCu with a 80/20 weight ratio, surrounded by a PTFE nozzle. Dimensions were derived in [7]. The closing motion is implemented via a pneumatic drive. Contact system and nozzle are enclosed in a pressure-tight vessel of 0.15 m^3.

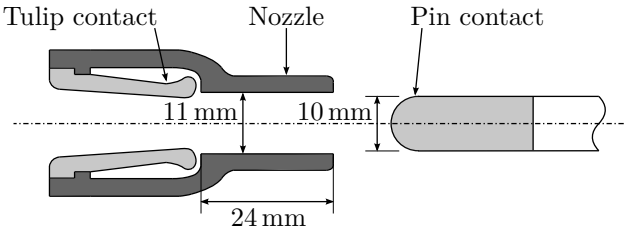

Figure 3. Section of the model load break switch.

Contact distance at the moment of arc ignition d is calculated based on travel signal measurement and contact geometry (Figure 4).

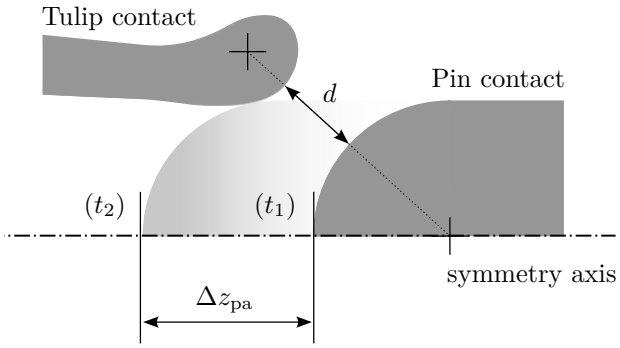

Figure 4. Contact distance at the moment of arc ignition (d) and distance traveled (Δz_{pa}) by moving contact during t_{pa}.

2.3. Underpressure during current making

For a successful current interruption, puffer-type LBSs rely on the cooling power provided by compressed gas. A compression (puffer) chamber generates the required pressure build-up during contact separation. Compressed gas is blown towards the switching chamber, cooling down the arc. In contrast, the closing motion during current making leads to expansion of the puffer volume, as shown in Figure 5. The resulting pressure drop between the contacts Δp is expected to have a negative influence on the dielectric strength of the medium [11], potentially leading to longer pre-strike interval. Since the DUT used in this paper does not include a puffer volume, an alternative approach for implementing Δp is needed.

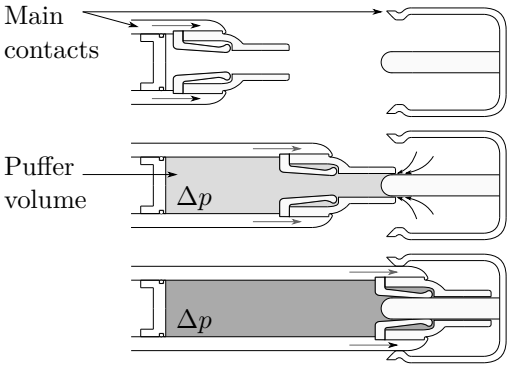

Figure 5. Expansion of puffer volume in a LBS during current making.

2.3.1. Implementation approach

Two different approaches were considered. The first approach consists of adjusting the nominal filling pressure p_f according to the expected Δp. The resulting adjusted filling pressure is $p'_f = p_f - \Delta p$. For the second approach, an external tank is used to generate a pressure gradient and realize the required Δp. External tank and main vessel are connected via a magnetic

valve, which is opened shortly before contact closing is initiated.

Expected Δp values for different closing speeds were calculated with a computational fluid dynamics (CFD) model, using a commercial software. Figure 5 shows the resulting relative pressure drop between the contacts during closing movement of a puffer-type LBS, under no consideration of the pre-strike arc. The model geometry is based on the DUT used for this contribution.

Pressure values measured at the point of galvanic contact (Table 3) were used as reference towards implementing Δp in the experimental setup. The Δp expected in a real puffer-type LBS is lower, since pre-strike arc is ignited in the range of ms before the point of galvanic contact (before $\times$ in Figure 6). The time difference depends on the conditions influencing the dielectric strength of the medium. The chosen Δp values result in a lower absolute pressure, and thus, lower dielectric strength compared to the real application.

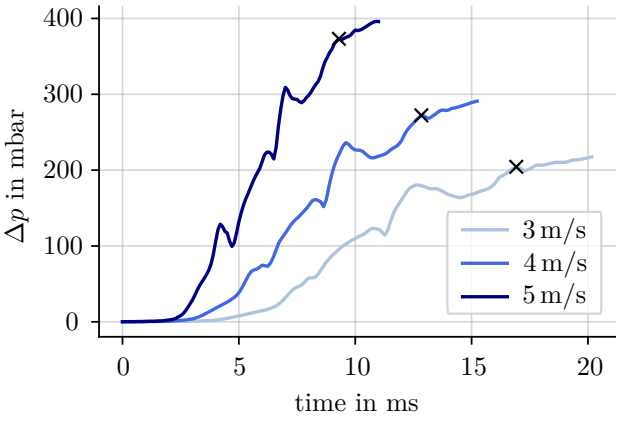

Figure 6. Simulated Δp during current making (time of galvanic contact represented by $\times$)

v_c in m/s	1	2	3	4	5
Δp in mbar	40	120	210	270	360

Table 3. Simulated pressure drop at the moment of galvanic contact in a puffer-type LBS.

Both approaches were experimentally tested following the method described in Section 2.1 for two v_c levels (3 and 5 m/s). Resulting t_{pa} were compared with the reference case where p_f is used under no consideration of Δp (Figure 7).

2.3.2. Comparison

For $v_c = 3$ m/s, median t_{pa} are 2.62 ms or 2.63 ms respectively when adjusted filling pressure p_f' or external tank are implemented. This represents a 12 % increase with respect to reference measurement (2.32 ms). For 5 m/s, the resulting t_{pa} are 1.73 ms (p_f') and 1.82 ms (ext.Δp), which represent a 19 - 24 %, respectively from the reference measurement (1.39 ms). Similar results are obtained using both approaches. Nevertheless, implementing Δp with an external vessel requires manual adjustment of filling pressure in the main vessel and external tank before performing each current making test, potentially leading to filling pressure deviations. To avoid this source of error, p_f' was used in the following.

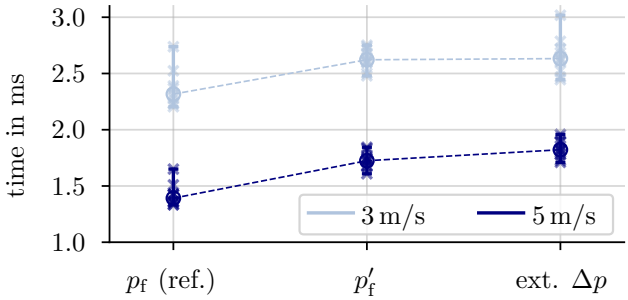

Figure 7. Pre-strike arc duration for $v_c = \{3, 5\}$ m/s using different Δp implementation approaches (individual test results and median represented by $\times$ and $\circ$, respectively).

A Keller Leo 2 digital precision manometer is used to set the filling pressure of the vessel containing the contact system to $p_f' \pm 4$ mbar.

3. Results and discussion

In Figure 8, the median response of t_{pa} and d for low, middle and high levels of v_c, p_f and r_{CO2} are depicted. The closing speed has the strongest influence on t_{pa} among the investigated parameters (Figure 8). In particular, stronger arcing time reductions can be achieved in the lower v_c region (between 1 m/s to 3 m/s). On the other hand, p_f has the strongest influence on d. In both cases, variations in % of CO_2 in the N_2/CO_2 mixture result in the smallest variation of t_{pa} and d for the investigated range.

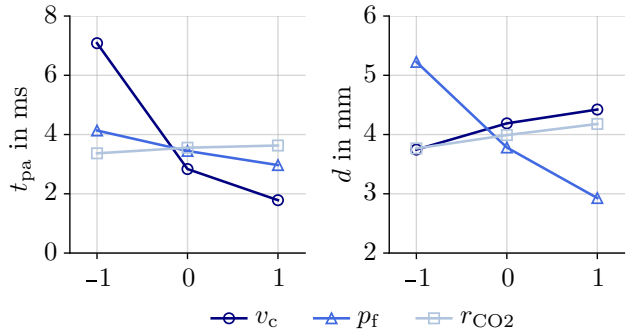

Figure 8. Main effects plots of median t_{pa} (left) and d (right), where $\{-1, 0, 1\}$ correspond to low, middle and high levels for v_c ($\{1, 3, 5\}$ m/s), p_f ($\{1.4, 1.8, 2.2\}$ bar) and r_{CO2} ($\{10, 40, 70\}$ % CO_2)

A closer examination of t_{pa} as a function of v_c and p_f is shown in Figure 9. A fast decrease in t_{pa} can be observed between 1 and 2 m/s, with further v_c increases leading to smaller t_{pa} reductions. This behavior is explained by an inversely proportional

relation of t_{pa} with v_c.

$$t_{pa} = \frac{\Delta z_{pa}(v_c)}{v_c} \tag{2}$$

where Δz_{pa} is the distance traveled by the moving contact during the pre-strike interval (see Figure 4). Due to expansion of the puffer volume, Δz_{pa} is dependent on v_c, with faster closing speeds leading to longer Δz_{pa} and d for the same filling pressure. This effect is also depicted in the main effects plot for d (Figure 8, right).

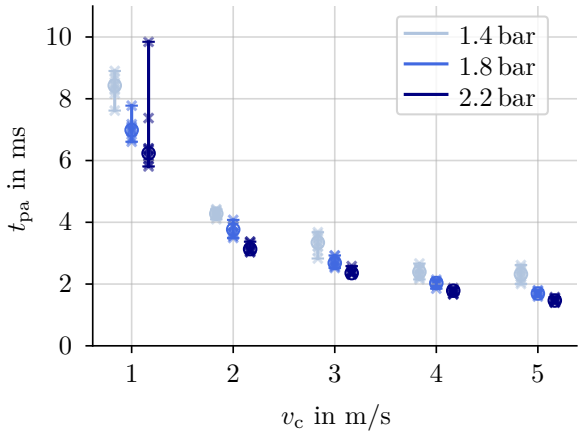

Figure 9. Pre-strike arc duration for $r_{CO2} = 40\,\%$. Individual test results and median represented by × and ○, respectively. Data points at different p_f values distributed around target v_c for visualization purposes.

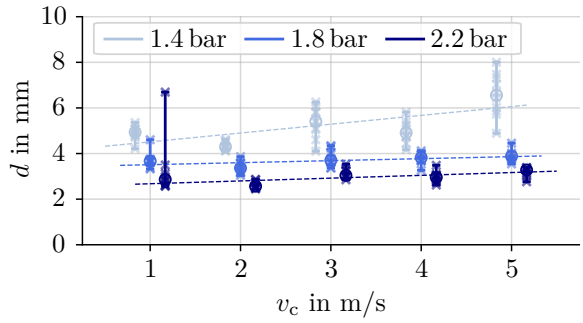

Figure 10. Contact distance at the moment of breakdown for $r_{CO2} = 40\,\%$. Individual test results and median represented by × and ○, respectively (dashed lines represent a least squares linear regression).

An increasing tendency of d over v_c can be observed in Figure 10. The steepest rate of rise is found for the lowest investigated p_f (1.4 bar). This can be explained by the absolute pressure drop due to Δp, relative to nominal filling pressure. Consider the implemented pressure drop at 5 m/s, $\Delta p_{(5\,m/s)} = 360$ mbar (Table 3). The resulting absolute pressures for the two extreme p_f cases are $p'_{f(1.4\,bar)} = 1.04$ bar and $p'_{f(2.2\,bar)} = 1.84$ bar, which represent a 25.7% and 16.4% deviation from the nominal filling pressure, respectively. The bigger relative drop in absolute pressure for the same closing speed may explain why contact distance at the moment of pre-strike arc ignition increases with closing speed at a higher rate for lower filling pressure.

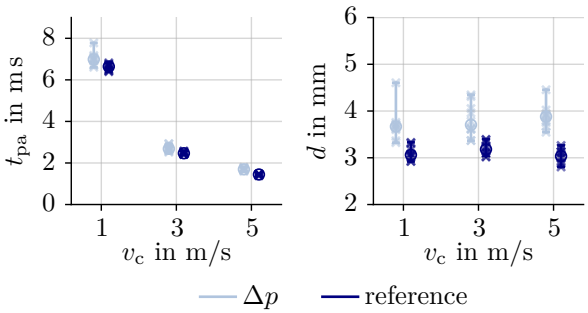

Figure 11. Comparison of t_{pa} and d when Δp is not considered (reference) for $p_f = 1.8$ bar, $r_{CO2} = 40\,\%$. Individual test results and median represented by × and ○, respectively.

To further illustrate the influence of puffer volume expansion on pre-strike arc, parameter variations using $p_f = 1.8$ bar and $r_{CO2} = 40\,\%$ CO_2 were repeated under no consideration of Δp. In Figure 11 and Table 4, no relevant variation of d_r is observed for increasing v_c. In contrast, adjusting the filling pressure results in longer contact distances, with faster closing speeds leading to stronger deviations from d_r. Similarly, $t_{pa,r}$ is higher than t_{pa} for every closing speed level, with faster v_c leading to bigger relative deviations from $t_{pa,r}$.

	1 m/s	3 m/s	5 m/s
d_r	3.06	3.18	3.03
d	3.67 (19.8%)	3.71 (16.5%)	3.88 (27.9%)
$t_{pa,r}$	6.64	2.47	1.45
t_{pa}	6.99 (5.2%)	2.68 (8.7%)	1.69 (17.1%)

Table 4. Comparison of median d and t_{pa}. $t_{pa,r}$ and d_r correspond to reference values under no consideration of Δp ($p_f = 1.8$ bar, $r_{CO2} = 40\,\%$)

Figure 12 shows the breakdown field strength for varying r_{CO2}. Considering the overlap between scattering of results across different variations, it can be concluded that mixing ratio in N_2/CO_2 mixtures is the least relevant of the investigated parameters towards reducing pre-strike arc duration. A linear increase of E_{bd} with p_f is achieved at constant r_{CO2}.

Figure 13 shows the prospective arc energy normalized to peak current. By increasing v_c from 1 to 2 m/s, a 58 – 69 % arc energy reduction can be achieved depending on p_f. Increasing v_c above 2 m/s leads to smaller arc energy reductions, and overlapping areas between subsequent v_c steps become wider. This effect, which becomes most evident for 4 and 5 m/s, indicates that increasing v_c beyond 5 m/s may result in only marginal reductions of t_{pa} and dissipated energy.

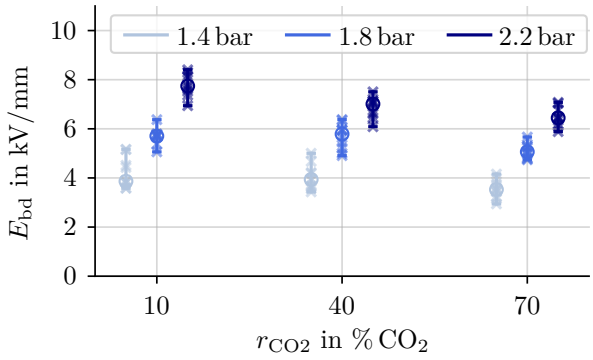

Figure 12. Breakdown field strength for different mixing ratios and $v_c = 3\,m/s$. Individual test results and median represented by × and ○, respectively. Data points at different p_f values distributed around target r_{CO2} for visualization purposes.

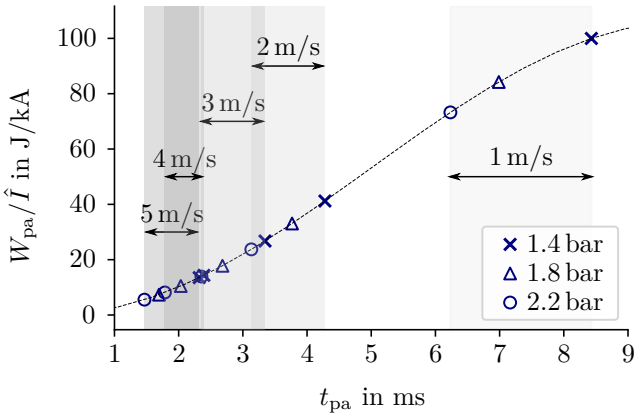

Figure 13. Prospective arc energy calculated using median t_{pa} values, for $r_{CO2} = 40\,\%$ ($\hat{I}$ represents peak value of symmetric short-circuit current).

4. Conclusion and Outlook

Closing speed is the most influential of the parameters investigated towards reducing pre-strike arc duration, followed by filling pressure. In particular, the most significant reductions in t_{pa} can be achieved when v_c is increased within the lower range (that is, 1 m/s to 3 m/s). Increasing the closing speed beyond 4 m/s results in comparatively small improvements. Expansion of the puffer volume during current making further limits the benefits of implementing faster closing speeds, which may not justify the challenges associated to installing a drive system capable of realizing such rapid closing operations. The percentage of CO_2 in N_2/CO_2 gas mixtures is the least influencing parameter, with lower CO_2 content leading to slightly better dielectric strength.

Contact degradation due to the short-circuit current making process is expected to have an influence on subsequent operations. Therefore, high-current testing is necessary to fully characterize the SCCM process. The findings obtained in this contribution will be applied in future work to evaluate contact degradation resulting from pre-strike arc. For this purpose, a test circuit enabling the generation of symmetric short-circuit currents will be implemented. The influence on contact degradation of parameters identified in this contribution as relevant will be experimentally characterized.

References

[1] G. Myhre, D. Shindell, F. M. Bréon, et al. *Anthropogenic and natural radiative forcing: Climate change 2013: The physical science basis. Contribution of working group I to the fifth AR of the IPCC.* Cambridge University Press, 2013.

[2] M. Bendig. *Ausschaltvermögen von Mittelspannungs-Lasttrennschaltern bei Verwendung atmosphärischer Lösch-und Isoliergase.* PhD thesis, RWTH Aachen University, Germany, 2020.

[3] N. Dorraki and K. Niayesh. Optical investigation on pre-strike arc characteristics in medium-voltage load break switches. *Journal of Physics D: Applied Physics*, 54(25):255503, 2021. doi:10.1088/1361-6463/abf25a.

[4] N. Dorraki, M. Strand, and K. Niayesh. Impact of pre-strike arc on contacts degradation after short circuit current making operation in medium voltage air load break switches. *30th International Conference on Electrical Contacts (ICEC 2020)*, 2021.

[5] N. Dorraki and K. Niayesh. An experimental study of short-circuit current making operation of air medium-voltage load break switches. *IEEE Transactions on Power Delivery*, 37(6):4646–4656, 2022. doi:10.1109/TPWRD.2022.3153237.

[6] M. Bendig, T. Krampert, N. Götte, et al. Investigations on the effect of the nozzle material on the interruption capability of a medium voltage load break switch. *PLASMA PHYSICS AND TECHNOLOGY*, 6(1):15–18, 2019.

[7] M. Bendig and M. Schaak. Design rules for environmentally friendly medium voltage load break switches. *IEEE Transactions on Power Delivery*, pages 1–9, 2020.

[8] T. Krampert, M. Bendig, A. Moser, and M. Schaak. Influence of the filling gas mixture on the interruption capability of medium voltage load break switches. *Plasma Physics and Technology*, 8(2):19–22, 2021. doi:10.14311/ppt.2021.2.19.

[9] J. Tepper, M. Seeger, T. Votteler, et al. Investigation on erosion of Cu/W contacts in high-voltage circuit breakers. *IEEE Transactions on Components and Packaging Technologies*, 29(3):658–665, 2006. doi:10.1109/TCAPT.2006.880476.

[10] Y. Yokomizu, T. Matsumura, R. Henmi, et al. Total voltage drops in electrode fall regions of SF_6, Argon and air arcs in current range from 10 to 20000 A. *Journal of Physics D: Applied Physics*, 29(5):1260–1267, 1996. doi:10.1088/0022-3727/29/5/020.

[11] N. M. B. Sham, N. Z. Zahid, M. S. Kamarudin, et al. Breakdown characteristic of N_2-CO_2 gas mixtures under AC and DC test voltages. *Journal of Physics: Conference Series*, 1874(1):012027, 2021. doi:10.1088/1742-6596/1874/1/012027.